Fermilab FERMILAB-TM-2221 September 2003

Radiation Load to the SNAP CCD

N.V. Mokhov, I.L. Rakhno, S.I. Striganov, T.J. Peterson

Fermilab, P.O. Box 500, Batavia, IL 60510, USA

October 13, 2003

Abstract

Results of an express Monte Carlo analysis with the MARS14 code of radiation load to the CCD optical detectors in the Supernova Acceleration Project (SNAP) mission are presented for realistic radiation environment over the satellite orbit.

1 Introduction

The purpose of the Supernova Acceleration Project (SNAP) is probing dark energy by observations of Type Ia supernovae in a 3-year space-based mission [1]. One of the crucial technical issues is radiation load to the critical devices, a charge-coupled device (CCD) photodetector first of all. It is calculated here with the MARS14 code [2] for a simple geometry model and radiation environment averaged over the SNAP orbit.

2 Radiation Environment at the SNAP Orbit

The orbit of the satellite (inclination 26.3 degrees, apogee 152830 km, perigee 10000 km) is taken into account by means of the codes CREME96 [3] and SPENVIS [4]. SPENVIS is used to represent electron component of Earth's radiation belts while CREME96 is used to represent galactic cosmic rays (GCR) and solar flares. The most significant limitation consists of the maximum apogee allowed in the code CREME96, namely 100000 km. Therefore the contribution from GCR is calculated here for a restricted orbit with apogee of 100000 km. All the spectra of incoming radiation are calculated taking into account geomagnetic shielding in the Earth's geomagnetic field.

The codes used allow us to divide the cosmic radiation into four categories:

1. Protons trapped in radiation belts.
2. Electrons trapped in radiation belts.
3. Primary (non-trapped) protons and heavy ions.
4. Primary (non-trapped) electrons.

Calculated orbit-averaged energy spectra for these components are shown in Figs. 1, 2 at solar minimum and at the largest solar flare. The contribution from primary electrons is taken from Ref. [5]. One sees that trapped protons and electrons and primary protons and α-particles are the drivers and needed to be taken into account as a source term. All these components but α are included in the MARS14 simulations and results are presented below.

Regular variations in solar activity during a so-called "11-year cycle" give rise to variations in integral particle fluxes of GCR within a factor of 2 while the variations in their spectra in the energy range of 10 to 1000 MeV can be more significant. At solar flares the number of protons emitted from Sun can increase significantly thus disturbing Earth's magnetosphere. It gives rise to variations in orbit-averaged fluxes for both trapped particles and GCR. The GCR spectra for the largest solar flare ever observed (October 20, 1989) [3] are shown in Fig. 2. For more realistic estimate of absorbed dose, a model of ordinary solar flares of a lower magnitude should be taken into account.

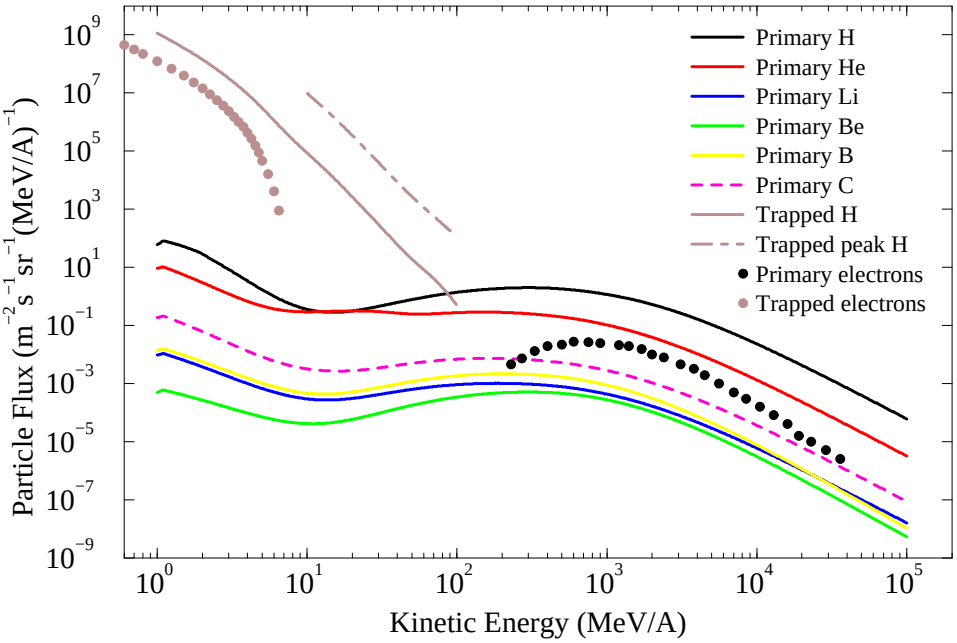

Figure 1: Orbit-averaged particle spectra, except "trapped peak", at solar minimum. The highest level of trapped protons ("trapped peak") is observed on a segment of the orbit near its perigee.

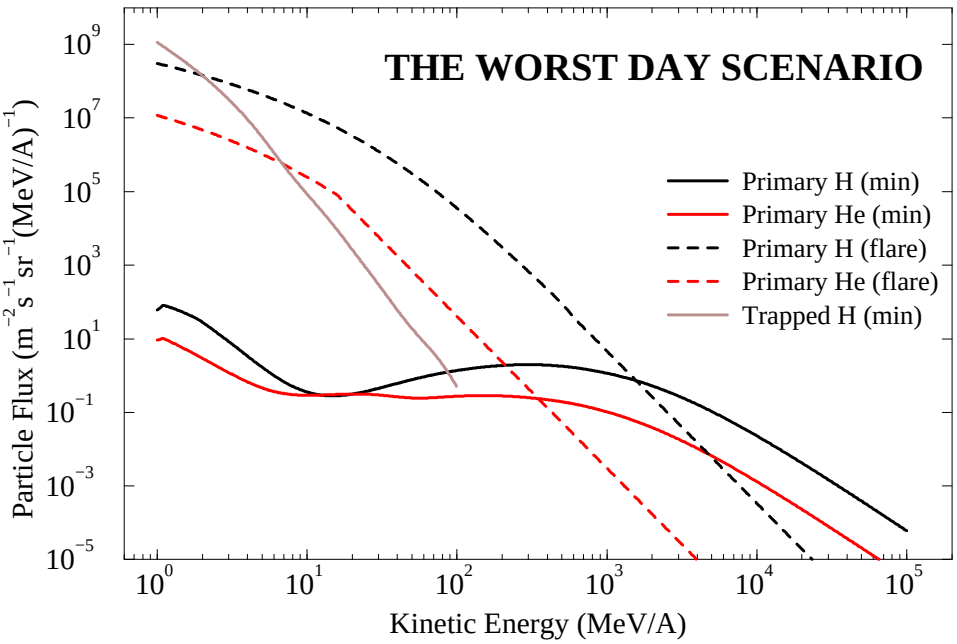

Figure 2: Orbit-averaged particle spectra at the largest solar flare ever detected.

3 Geometry and MARS Modeling

Calculations of radiation exposure of a SNAP CCD were performed for the orbit described above. Hadronic and electromagnetic showers induced in the apparatus by the sources described in the previous section are simulated with the MARS14 code in the energy range from 100 GeV down to 0.1 MeV.

In order to simplify the radiation model, a judgment was made regarding which parts of the SNAP satellite would be the most significant in terms of intercepting incoming cosmic radiation. Information about the SNAP conceptual design was obtained from the file *S-14_full_assy.SLDASM* in *full_assy_model_e_test*, downloaded from the LBNL engineering website [6]. The material through which a particle from the sun-side would pass would most likely consist of, at minimum ("minimum" since lots of other smaller items on the spacecraft and attached to the optical bench may also be encountered):

- Multi-layer insulation (MLI) consisting of 30 layers of about 6-micron thick mylar, at a density of 15 layers per cm, each layer coated on both sides with about 500 Å of aluminum. The MLI also includes a very low-density spacer (polyimide) between layers of mylar.
- The optical bench, consisting of layers of 2-mm thick carbon-fiber "tooling plates".
- The conical shield, material and thickness to be optimized within mass, space, structural and thermal constraints.

A few things are added to the above items in front, depending on the angle of approach:

- The spacecraft deck (if the angle is from below) consisting of two layers of carbon-fiber composite 1-mm thick each and a 51-mm thick layer of aluminum foils.
- If the angle is from above, one has the following sequence: MLI, baffles (which are 1-mm thick aluminum), main mirror, optical bench box, and shield.

From the side opposite the Sun the situation is quite different; the thermal radiator is the main piece of material and appears to be essentially the only material. The present thermal radiator concept is 1.25-cm thick aluminum.

For this model, we begin with just the spacecraft deck, thermal radiator, optical bench box, conical shield, and the cold plate supporting the CCD array. A simplified geometry model used in the simulations is shown in Figs. 3 through 5. The satellite axis is along the z-axis. The three-layer deck is modeled according to the description given above. The optical bench box is assumed to be made of the carbon-fiber composite with thickness equal to 2 mm. The conical shield is modeled as an aluminum cone 2-cm thick. The cold plate is modeled as a molybdenum hexagon 2.5 cm in thickness. The opening in the optical bench box for incoming optical radiation is modeled as a circular (R=30 cm) hole in the box (in xz-plane) with a center at y = -63 cm and z = 75 cm (Fig. 3). The array of CCD photodetectors is modeled as a 200-μm thick silicon disk placed on a substrate (Fig. 3).

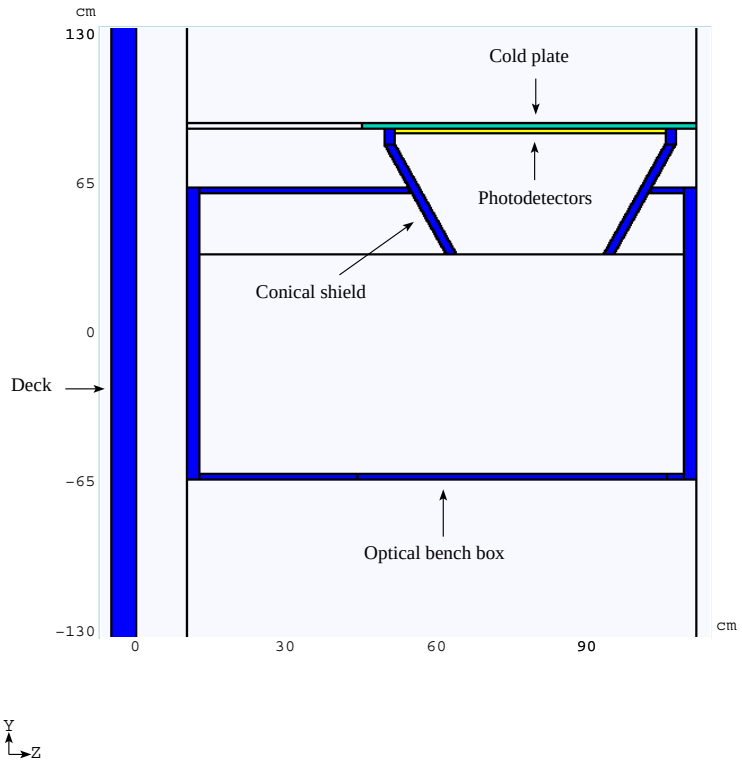

Figure 3: A fragment of the satellite MARS model (yz-view).

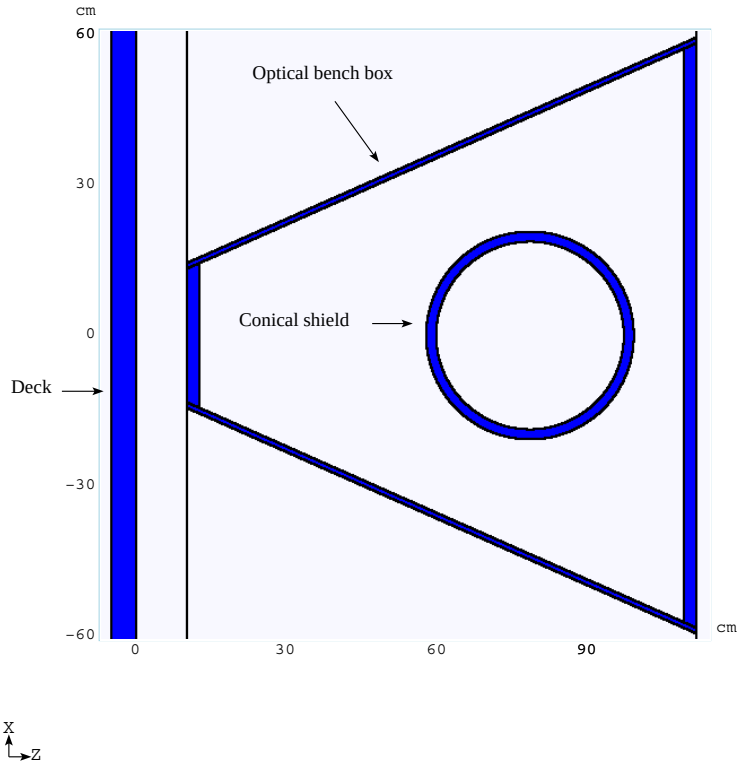

Figure 4: A fragment of the satellite MARS model (xz-view).

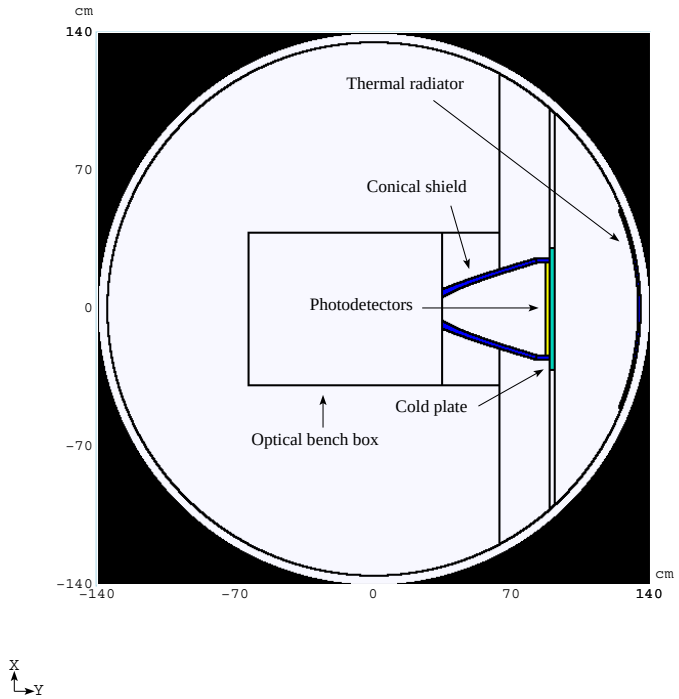

Figure 5: A fragment of the satellite MARS model (xy-view).

4 Particle Spectra and Dose Accumulated in CCD

In Monte Carlo calculations performed with the MARS14 code, the satellite is not considered to be orientation-stabilized and all the source terms are assumed to be isotropic. Three cases are considered:

1. Solar activity at minimum.
2. Solar activity at maximum.
3. The worst day scenario: the largest solar flare ever observed.

Two-dimensional distributions of particle fluxes over the system are given in Figs. 6 through 11 for two sources of space radiation: galactic protons and protons trapped in radiation belts. The distribution of high-energy galactic protons in the region is practically isotropic (see Fig. 6) and demonstrates the well-known level of about 4 particles/cm^{2}s [7]. Secondary neutrons are generated by galactic protons mostly in the cold plate, thermal radiator, and spacecraft deck (see Figs. 7 through 9). The most important contribution to neutron flux in the vicinity of the CCD photodetector is due to the cold plate.

Neutron generation by low-energy protons trapped in the radiation belts is significantly lower than that due to galactic protons and occurs mostly on the thermal radiator and deck as can be seen in Figs. 10 and 11. Also Fig. 10 shows that the thermal radiator serves as an absorber of the low-energy trapped protons but not as a generator of secondary hadrons (the same is true for the deck). One can expect a higher absorbed dose in the CCD photodetector due to trapped protons when compared to that due to galactic protons because of a signif-

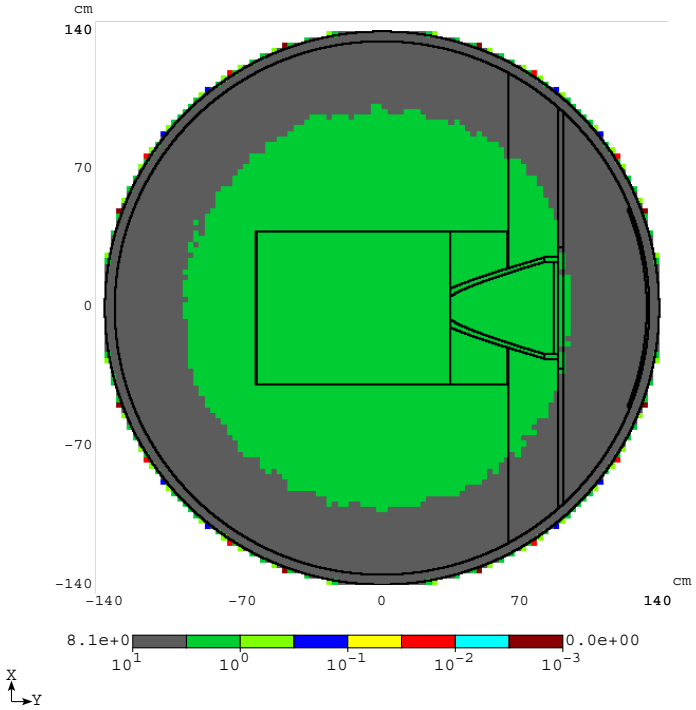

Figure 6: Charged hadron flux isocontours ($cm^{-2}s^{-1}$) in the model (xy-view) due to galactic protons.

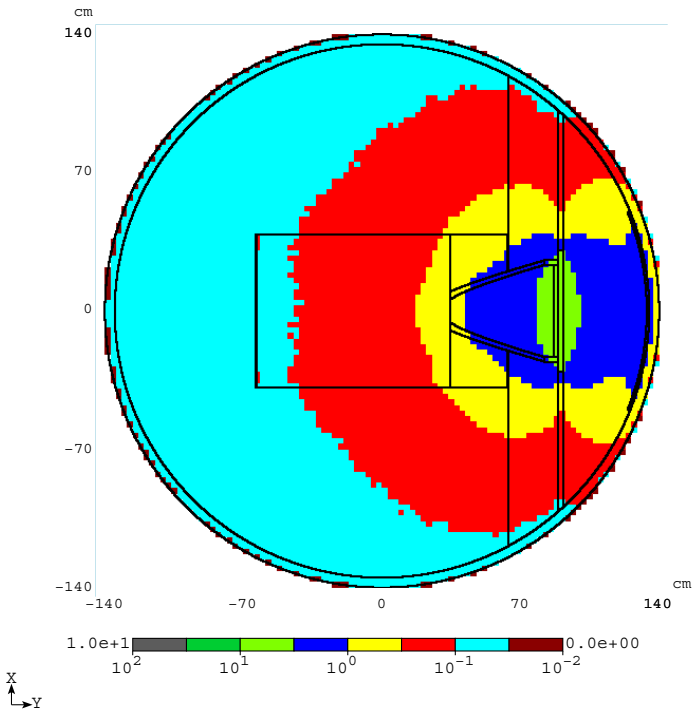

Figure 7: Neutron flux isocontours ($cm^{-2}s^{-1}$) in the model (xy-view) due to galactic protons.

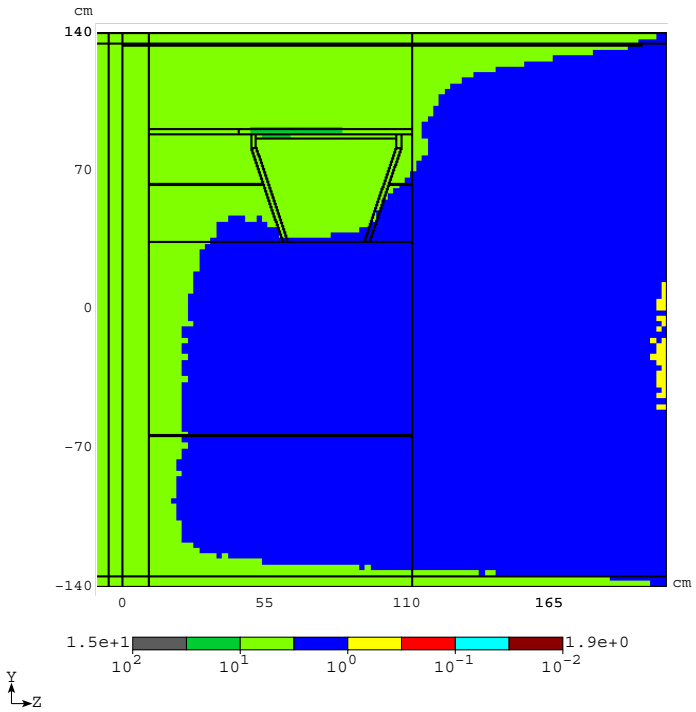

Figure 8: Total hadron flux isocontours ($cm^{-2}s^{-1}$) in the model (yz-view) due to galactic protons.

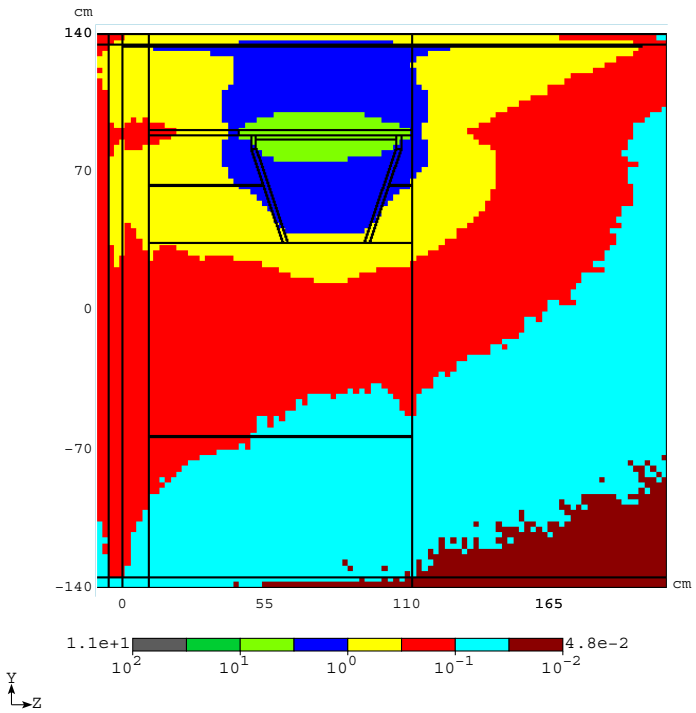

Figure 9: Neutron flux isocontours ($cm^{-2}s^{-1}$) in the model (yz-view) due to galactic protons.

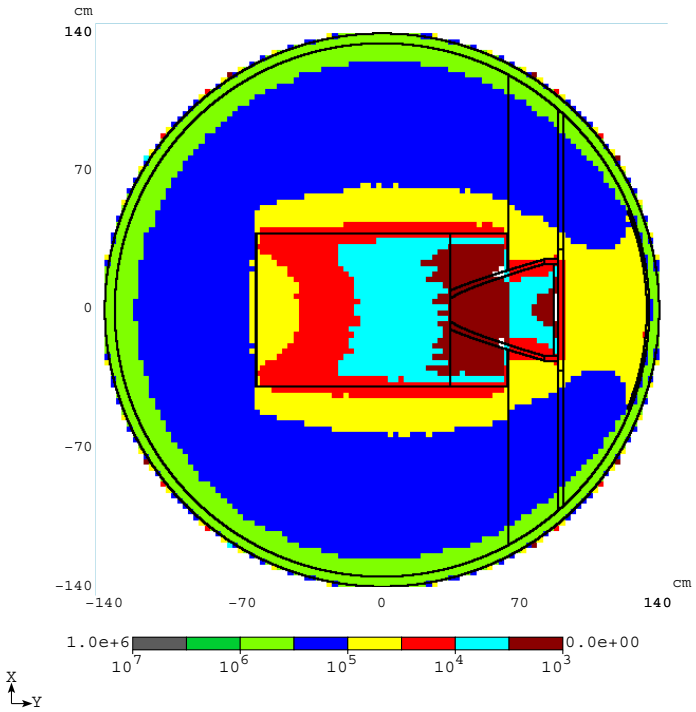

Figure 10: Total hadron flux isocontours ($cm^{-2}s^{-1}$) in the model (xy-view) due to protons trapped in radiation belts.

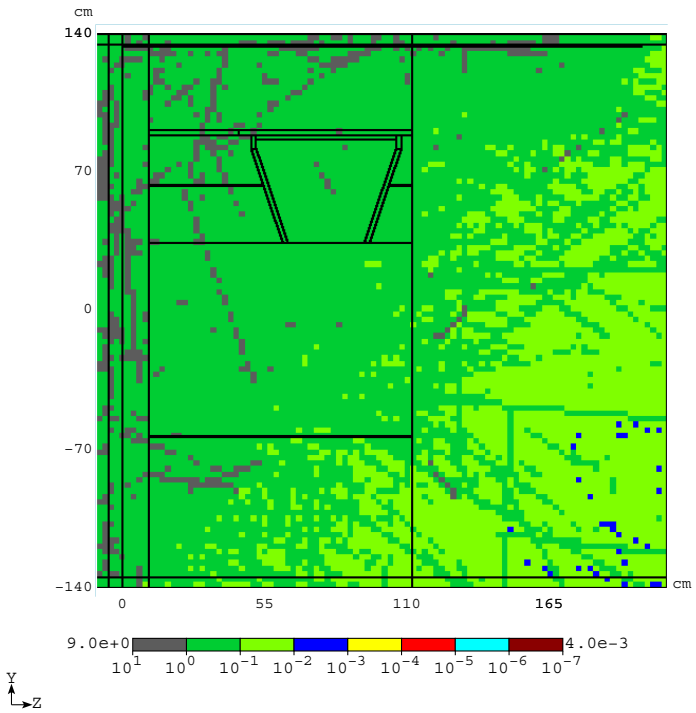

Figure 11: Neutron flux isocontours ($cm^{-2}s^{-1}$) in the model (yz-view) due to protons trapped in radiation belts.

icant difference of the hadron fluxes in the vicinity of the photodetector — approximately 10^3 and 10 $cm^{-2}s^{-1}$, respectively.

The dose absorbed in the CCD during the worst day due to the largest solar flare equals to 4 rad, *i.e.* about 50% of the yearly dose due to primary protons at solar minimum (see Table 1).

Table 1: Yearly absorbed dose (rad) in CCD.

Radiation source	Absorbed dose
Primary protons	7.9
Primary electrons	0.3
Primary α-particles$^{(*)}$	3.2
Trapped protons	20700
Trapped electrons	7750
Total	28460

$^{(*)}$ Estimation (see next section).

5 Verification

The CREME96 code [3] includes, in particular, routines for estimation of radiation attenuation by a shielding layer and absorbed dose in a silicon target. One of the routines, TRANS, keeps track of nuclear fragments produced by cosmic-ray projectiles. The routine, however, does not track low-energy and short-range fragments produced from target nuclei in shielding material itself. The results can be used for comparison with the detailed MARS calculations above.

Using the CREME96 built-in routines, we estimated absorbed dose in a silicon target shielded with a 3-cm aluminum layer. The yearly dose in such a target due to primary protons equals to 4.7 rad according to CREME96 and should be compared to the value of 7.9 rad in Table 1. Taking into account all the differences between the two models (simplified shielding in CREME96, different sensitive elements and different physical models employed for particle interactions and transport in the two codes) the agreement is quite reasonable.

An estimate of the absorbed dose in a silicon shielded with a 3-cm aluminum layer was performed by means of CREME96 for a combined effect of primary protons and α-particles. The yearly dose is up by 40% becoming 6.5 rad. Thus, taking α-particles into account is mandatory for orbits and models where/when the contribution from primary cosmic rays dominates over that from the trapped protons.

6 Estimate of Charge Transfer Efficiency Degradation

Degradation of charge transfer efficiency (CTE) due to radiation damage is a major concern for such highly sensitive photodetectors as CCD. Table 2 gives predicted CTE degradation based on an approximate separation of energy deposited in the detector into the ionizing and non-ionizing energy loss (NIEL). It is NIEL that gives rise to atomic displacements and generation of effective charge traps responsible for the CTE degradation. For estimate, we used the fact that 1 rad is approximately equivalent to 10^{-3} non-ionizing rad (*nirad*) for proton radiation in such an environment [8, 9]. For neutrons NIEL is less than that for protons at the same energy in the region from 100 keV up to 10 GeV while for electrons NIEL is less than that for neutrons, at least, by a factor of ten [10]. Taking all that into account and using the data from Table 1, one obtains the yearly non-ionizing absorbed dose in the CCD of about 20.7 nirad (only major radiation contribution due to trapped protons is considered). Further, we used the degradation rates specific to the two best devices developed at LBNL: standard high-resistivity devices and notch high-resistivity devices with ΔCTE equal to $2.5{\cdot}10^{-13}$ and $9.6{\cdot}10^{-14}$ g/MeV, respectively [11]. Other devices have significantly higher degradation rates [11] and are not considered in the paper.

Table 2: Predicted degradation (%) of performance of the CCD photodetector with $1024{\times}1024$ pixels for a 4-year mission. The optimistic and pessimistic estimates refer to ΔCTE equal to $9.6{\cdot}10^{-14}$ and $2.5{\cdot}10^{-13}$ g/MeV, respectively. The degradation was calculated as 1 - CTE^{1024}.

Radiation source	Optimistic estimate	Pessimistic estimate
Trapped protons	40	73

One can see that the predicted CTE degradation even for the LBNL notch high-resistivity devices is significant while other ones can hardly survive for the 4-year mission.

7 Conclusions

The analysis performed enabled us to get the first estimate of radiation load to the SNAP CCD in a simplified geometry model and for the realistic radiation environment on the orbit. The following items should be refined in further studies:

1. Allowable limits for the CCD and electronics – radiation dose, total fluxes and background rates – to design shielding appropriately.
2. CCD specific: charge transfer efficiency *vs* accumulated dose.
3. Add more realism to the CCD detector model.
4. Add other components of the satellite.

5. Add and analyze on-board electronics that needs protection against radiation.

6. Clarify details (position, dimensions etc) of the opening in the optical bench box for incoming optical radiation.

7. Add accurate treatment of transport and interactions of α-particles and possibly heavier ions.

8. Date of the beginning and duration of the mission; it is required to take into account a model of regular solar flares.

8 Acknowledgments

We are thankful to Fritz DeJongh for detailed info on orbit parameters, Peter Limon for useful comments as well as Chris Bebek, Robin Lafever, and Robert Besuner of LBNL for valuable info on used materials.

References

[1] http://snap.lbl.gov/

[2] N.V. Mokhov, "The MARS Code System User's Guide", Fermilab-FN-628 (1995); N.V. Mokhov, O.E. Krivosheev, "MARS Code Status", Proc. Monte Carlo 2000 Conf., p. 943, Lisbon, October 23-26, 2000, Fermilab-Conf-00/181 (2000); N.V. Mokhov, "Status of MARS Code", Fermilab-Conf-03/053 (2003); http://www-ap.fnal.gov/MARS/.

[3] https://creme96.nrl.navy.mil/

[4] http://www.spenvis.oma.be/spenvis/

[5] M. Aguilar *et al. Phys. Rep.* **366** (2002) 331-405.

[6] http://www-eng.lbl.gov/ hoff/

[7] Alan C. Tribble, "The Space Environment. Implications for Spacecraft Design", Princeton, New Jersey, Princeton University Press, 1961, p. 148.

[8] J.E. Nealy, G.D. Qualls, L.C. Simonsen, "Integrated shield design methodology: application to a satellite instrument", in Proc. NASA Workshop on shielding strategies for human space exploration, Houston, Texas, December 6-8, 1995; NASA Conference Publication 3360, December 1997, p.385-396.

[9] G.R. Hopkinson, C.J. Dale, P.W. Marshall, "Proton Effects in Charge-Coupled Devices", IEEE Trans. on Nucl. Sci., v. 43, #2 (1996), p.614-627.

[10] A.Holmes-Siedle and L.Adams, "Handbook of Radiation Effects", Second Edition, Oxford and New York, Oxford University Press, 2002, p.114.

[11] C. Bebek, D. Groom, S. Holland *et al.*, "Proton radiation damage in P-channel CCDs fabricated on high-resistivity silicon", http://snap.lbl.gov/pubdocs/CCDpaper_rev2.pdf